catalysts

MDPI

Article

In-situ Quantification of Nanoparticles Oxidation: A Fixed Energy X-ray Absorption Approach

Enrico Berretti [1], Andrea Giaccherini [2,3,7], Giordano Montegrossi [4,7], Francesco D'Acapito [5], Francesco Di Benedetto [3,7], Claudio Zafferoni [6], Alessandro Puri [5], Giovanni Orazio Lepore [5], Hamish Miller [1], Walter Giurlani [6], Massimo Innocenti [6,7], Francesco Vizza [1] and Alessandro Lavacchi [1,*]

1 Institute for the Chemistry of Organometallic Compounds, Italian National Research Council (ICCOM-CNR), 50019 Florence, Italy
2 Department of Industrial Engineering "DIEF", University of Florence, 50139 Florence, Italy
3 Earth Sciences Department, University of Florence, 50121 Florence, Italy
4 Institute of Geosciences and Earth Resources, Italian National Research Council (IGG-CNR), 50121 Florence, Italy
5 Operative Group Grenoble, Istituto Officina dei Materiali, Italian National Research Council (CNR-IOM-OGG) c/o European Synchrotron Radiation Facility (ESRF), F-38043 Grenoble, France
6 Chemistry Department, University of Florence, 50019 Florence, Italy
7 National Institute for Science and Technology of Materials (INSTM)—Research Unit of Florence, 50121 Florence, Italy
* Correspondence: Alessandro.lavacchi@iccom.cnr.it; Tel.: +39-055-522-5250

Received: 6 June 2019; Accepted: 28 July 2019; Published: 31 July 2019

Abstract: The oxidation of palladium nanoparticles causes the performance degradation of alkaline direct ethanol fuel cells. Quantifying this oxidation is a task of tremendous importance to design mitigation strategies that extend the service life of catalysts and devices. Here, we show that the Fixed Energy X-ray Absorption Voltammetry (FEXRAV) can provide this information with an in-situ approach. To do so, we have developed a quantification method that assumes the linear response at fixed energy. With this method, we have investigated the oxidation of carbon black-supported palladium electrocatalysts during cyclic voltammetry in the same solution employed as a fuel in the direct ethanol fuel cells. We have shown that up to 38% of the palladium is oxidised at 1.2 V vs. RHE and that such oxidation also happens at lower potentials that the catalyst can experience in real direct ethanol fuel cells. The result of this study is a proof of concept of quantitative FEXRAV.

Keywords: palladium; electrocatalysis; ethanol; X-ray Absorption Spectroscopy; FEXRAV

1. Introduction

Understanding electrocatalysts at work is a task of tremendous importance to design efficient fuel cells and electrolysers. This can be done by methods that investigate materials in their working environment under the application of an electrical potential difference. Among these techniques, X-ray Absorption Spectroscopy (XAS) plays a major role [1–4]. Three main reasons account for this: (i) XAS provides short-range structural information around a given element, shedding light on its valence state, and on distance, nature and number of neighbouring atoms [5]; (ii) High energy X-rays (e.g., Pd Kα ca. 24 keV) easily penetrate materials crossing the boundaries of the working environment with little attenuation and enabling the analysis of complex systems/matrices. The ability to reach a high flux/high energy X-Ray output also enables to scope out a wide array of elements; (iii) under appropriate circumstances (nanoparticles, thin films under grazing angle irradiation), XAS is sensitive

to surfaces and interfaces, a fact that is extremely important to understand the way in which materials interact with the environment.

Since the inception of high brilliance synchrotrons, in-situ XAS has unravelled surface and interphase phenomena in heterogeneous catalysis, electrocatalysis and more generally in materials science [6]. In these studies, chemical reactions and physical parameters such as temperature, pressure and, in the case of electrochemistry, potential, modify the surface composition and structure. This latter point is, at present, of paramount importance because of the role of electrochemistry in the conversion and storage of renewable energy. Fuel cells, batteries and electrolyser efficiency and functionality largely depend on the surface of the electrocatalytic materials that can deactivate by oxidation or the adsorption of poisoning chemical species.

Time-resolved XAS is a preferential choice to understand the nature and the dynamics of electrocatalyst deactivation processes. In many cases, such surface information also provides essential insights to understand the steps of electrochemical reactions catalysed by the surface [7–12]. So far, this aim has been afforded by quick-XAS. Quick XAS consists of a peculiar acquisition technique [13] not available in all beamlines, allowing the fast collection of XAS spectra in less than 1 s.

Minguzzi et al. have recently demonstrated a radically innovative approach to the XAS investigation of materials evolution [14–16]. This consists of the acquisition of the XAS signal at fixed energy (FEXRAV, Fixed Energy X-Ray Absorption Voltammetry), following the intensity of that signal with time during voltammetry. Under this setup, a signal variation can be interpreted as a change in the redox state and/or in the coordination of the absorber element, that is at least partially converted to a different species. The key point in this approach is the selection of the right fixed energies for the XAS measurements. This is done using the acquisition of X-ray Absorption Near Edge Spectroscopy (XANES) spectra on standards, i.e., compounds containing the element under investigation in different valence states. The reference compounds should be, as much as possible, representative of the species likely present under working conditions. Then, by comparing their XANES spectra, the energy exhibiting the largest variation among the reference spectra can be selected as the region with the highest achievable analytical sensitivity). Our quantification approach is based on the "lever rule", which implies the linear response of the signal due to change of the ratio between two phases (represented by the reference compounds) at fixed energy. This assumption is commonly considered very solid since the linear combination fit is the most common way to perform quantitative XANES analysis.

FEXRAV was applied for the first time to the study of the evolution of the Iridium speciation in Iridium oxides during cyclic voltammetry to unravel the chemical changes of Iridium in the oxygen evolution reaction [16]. Successively, the validity of the method was confirmed by the investigation of the chemical speciation of silver [15], copper [17] and iron [18] electrocatalysts.

These successful experiences showed the potential of FEXRAV as a practical analytical tool for investigation of electrocatalysts in the conditions encountered in real applications. However, a method for the quantification of FEXRAV data and their uncertainties are still missing. The determination of surface or interphase composition would be an extremely powerful quantitative tool able to deepen the knowledge of how electrocatalysts work and deactivate. Moreover, FEXRAV permits to work in-situ, directly inside the studied electrochemical wet system. This is an advantage in respect to other ex-situ techniques for surface characterisation, like XAS, in which samples have to be kept in high vacuum. The development of this quantitative approach to FEXRAV, as well as the identification of the speciation promoted during voltammetry, are the major objectives of this study.

To give a demonstration of our approach, we have defined a case study: this consisted of the analysis of the potential dependent palladium oxidation in an alkaline environment. The electro-oxidation of palladium in alkali is particularly relevant for its extremely high electrocatalytic activity, both toward alcohols and hydrogen oxidation [19–22]. This property has been widely exploited in direct ethanol fuel cells [23–26] and electrochemical reformers [27,28] both promising energy conversion and storage devices. Palladium also offers the advantage of having well-known chemistry in an alkaline environment that helps much in the selection of the best conditions to perform FEXRAV. Indeed,

Pd^0 is known to oxidise to Pd(II) oxides/hydroxides at pH larger than 13 for potential larger than 0.5–0.6 V vs. RHE [29,30] with no formation of Pd(IV) species. However, at higher potential palladium is also dissolved in the electrolyte [29,31–33], an aspect that is limited by the presence of reducing agents such as $NaBH_4$ [23] or even milder ones such as ethanol [34,35], ethylene glycol [36–38] and glycerol [38–40]. It is also known that only metallic Pd shows activity towards ethanol electrooxidation, while Pd(II) species are not electroactive toward this reaction [20]. Additionally, Pd electrocatalysts consists of Pd nanoparticles (5 nm [21,38]) dispersed onto black carbon support. The limited size of the particles provides a high surface to volume ratio and turns XAS into an in-situ technique sensitive to the chemical state of surface atoms, enabling the study the evolution of the speciation of an element among two oxidation states.

2. Results & Discussion

2.1. Nanoparticles Characterisation

The acquisition of surface-sensitive XAS spectra can be obtained either using grazing-incident techniques (GIXAS, ReflEXAFS [41]) or by studying samples consisting of very small particles (or thin films). This is required to have a high ratio between surface and bulk atoms, a condition that is usually met in nanoparticles (NP) with a diameter lower than 10 nm. To check if the catalyst employed in this investigation met this condition, we performed field emission scanning electron microscopy to determine particle size. Figure 1 reports the TEM and the SEM backscattered electron images taken on the catalyst at high magnification. Most of the particles are less than 5 nm, and many of them are below 3 nm assembled in well-defined clusters.

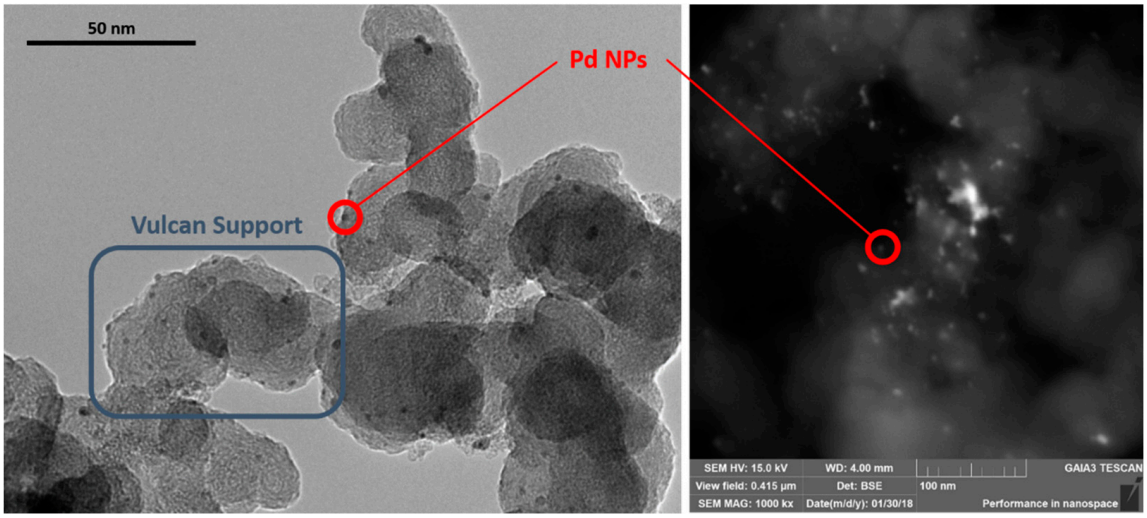

Figure 1. TEM (**left**) and Backscattered SEM (**right**) images of the Pd/C electrocatalyst. The backscattered images show Pd NPs as black spots (TEM) and white spots (SEM with an inverted contrast in respect to TEM), while the grey haloes come from carbon support.

XRD proved that particles are metallic Pd with a significant peak broadening due to the small size of the crystallites [42]. No peak related to crystalline Pd oxide was detected (Figure 2). However, from XRD, we cannot exclude the presence of a limited amount of amorphous oxide or hydrous oxide at the surface of the nanoparticles, especially if these phases occur in amounts below some wt% units in the sample. It is worth mentioning that a limited amount of these phases at the surface of Pd NP do not affect much catalytic activity [43].

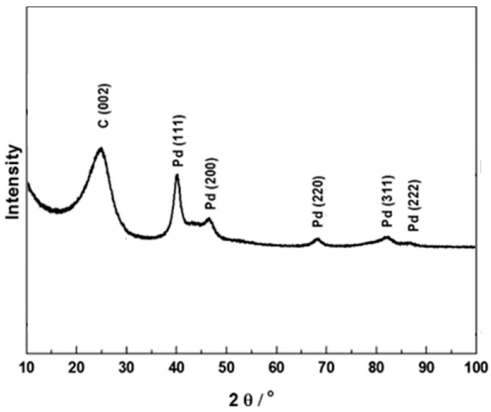

Figure 2. XRD spectra of the Pd/C catalyst employed in this work.

2.2. Design, Realisation and Testing of the Electrochemical Cell

To perform the FEXRAV experiments, we have designed a new dedicated electrochemical cell that fits the LISA beamline hardware set up, like already done by other groups [43]. Our cell is designed to acquire XAS spectra in the Fluorescence configuration, with a 45° angle between the normal to the working electrode (WE) surface and the axis of the incoming beam [31]. The cell consists of two main sections: (i) the cell head assembly and (ii) the cell body (Figure 3).

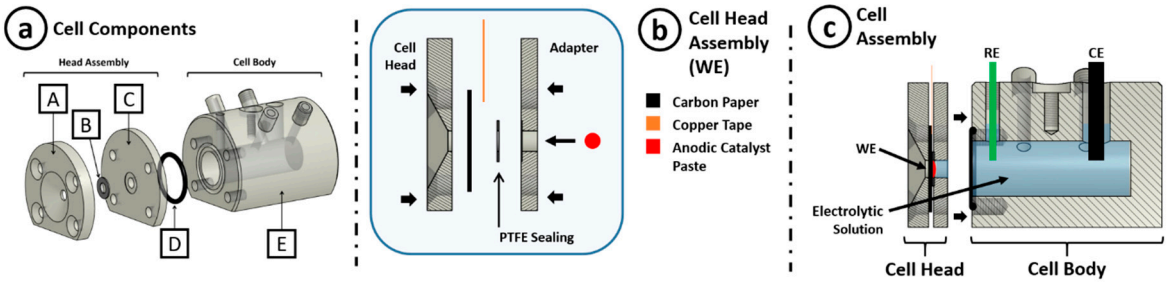

Figure 3. Experimental cell for Fixed Energy X-ray Absorption Voltammetry (FEXRAV) measurements at the K-alpha edge of Pd: (**a**) 3D ensemble view, depicting EC-cell components: A. Cell Head, B. PTFE sealing, C. Adapter, D. Sealing, E. Cell Body; (**b**) exploded section view of the cell head, (**c**) lateral section view of the assembled cell.

The cell head (Figure 3a, elements A, B and C) holds in place the WE (a Pd/C ink deposited onto carbon paper, as visible in Figure 3b), allowing the catalyst exposure to X-Rays from one side and the contact to the electrolytic solution on the other. Its assembly consists of a cap, a PTFE sealing, a spacer-adapter and of a carbon paper electrically connected to the potentiostat by a strip of conducting copper tape. The mass attenuation of the supporting carbon paper and the deposited ink is negligible [44]. This is essential to record the fluorescence signal that comes from the Pd NP in contact with the electrolyte. The carbon paper on which the catalyst is drop-casted, together with the PTFE sealing, prevent water flooding out from the X-ray window. It is worth mentioning that the carbon paper surface largely exceeds the size of the X-ray window, to allow the connection with the copper tape without shielding the X-rays. Four screws fix together the head cell assembly with the cell body, pressing the electrode and making the sealing tight. The cell head cap has a flaring hole that allows the X-rays coming from the electrodes to reach the detector for analysis in Fluorescence mode. The cell body E (Figure 3a) contains the electrolyte tank with the holes for positioning the reference electrode (RE) close to the WE surface, the counter electrode (CE) and the gas inlet and outlet (to keep the cell under a nitrogen atmosphere, Figure 3c). The tank is a cylinder with a diameter of 10 mm and a depth of 52 mm half-filled with electrolyte. Such a large volume has been intentionally selected to allow long experiments without significantly depleting the concentration of the electroactive species. Additionally, this avoids the use

of flow systems that complicate the experimental design and that are difficult to fit inside or in the surrounding of the experimental XAS chamber. To accurately position the X-ray window inside the chamber, the cell was fixed on a chamber holder allowing an x,y,z motion (laboratory reference system) together with the rotation (along the z-axis) required to set up the cell in Fluorescence configuration. All the cell components are made in polymethyl methacrylate (PMMA), apart from the PTFE sealing ring (B) and O-Ring (D), and the screws that we used to fix the head assembly to the cell body, made of steel. We choose to have an X-ray window of 5 mm diameter (on the cell head A, Figure 3a). This size was selected to fit the beam into the X-ray window easily. Successively, we defined a protocol for cell assembly and use, including the deposition of a known amount of catalyst exactly on the X-ray window.

2.3. XAS Analysis

The key for a successful FEXRAV acquisition is the selection of the best-fixed energy, chosen in order to maximise the analytical sensitivity as already mentioned in the introduction. Remarkably, palladium oxidation in alkaline media leads mostly to the formation of a thin layer of palladium (II) oxides or oxyhydroxides and Pd dissolution as hydroxy-palladiates [29,43]. In principle, the formation of these Pd(II) species is strongly dependent on the applied electrochemical parameters. This means that different NP sizes, subjected to the same oxidation stimulus, grow the same amount of Pd(II) species per surface unit. Indeed, on a single particle, the overall proportion between produced Pd(II) species (present on the surface) and the inmost metallic palladium atoms can vary depending on NP dimensions. Hence the maximum variation in the Pd(II)/Pd^0 ratio is also deeply dependent on the catalyst NP dimensional dispersion, while the XAS fluorescent intensity is related to their concentration in respect of the carbon powder.

Pd dissolution in bare alkali has been previously demonstrated by Pourbaix diagram calculation, XAS analysis and EQCM [20,31,45]. Liang et al. found that Pd oxidation happens with the formation of the same species even in ethanol containing electrolytes. In this case, Pd oxidation is known to compete with ethanol oxidation becoming faster with the increase of the potential. The advantage of using ethanol is that it limits the dissolution of Pd(II) species as ethanol is known to be a reducing agent for dissolved Pd [46].

We first acquired the reference spectra of pure Pd and pure PdO samples, to look for the proper energy to investigate palladium oxidation with FEXRAV. The choice of Pd and PdO as a standard is robust as the XANES spectrum of the electrochemically stressed palladium can be successfully fitted using these two chemical species [21,47]. Although a relevant aliquot of the Pd(II) species investigated by FEXRAV is probably $Pd(OH)_4^{2-}$ (due to the dissolution process already mentioned) the preparation of a reliable standard solution is impossible in the sense that it could affect the reproducibility of the measurements. Still, PdO and $Pd(OH)_4^{2-}$ share the same coordination geometry, number and distances and the same ligand species, showing the same features in the respective XAS spectra [47–52]. All this considered PdO should be considered the best standard for the XANES of $Pd(OH)_4^{2-}$. Figure 4a shows a series of spectra obtained by linearly combining the reference spectra in variable ratios. Standard energy scales were calibrated with an in-beam Pd foil in order to avoid uncompensated shifts of edge values. The fitting shows that two energies, respectively around 24,350 and 24,370 eV, display large spectral variation. Particularly, the intensity of the peak at 24,350 eV decreases when the oxide fraction increases, while that of the peak at 24,370 eV increases with increasing oxide content. Among the two, the peak at 24,370 eV shows the largest variation (Figure 4). Accordingly, we selected this energy value to monitor the change in the Pd speciation. However, in order to check that no other unpredicted chemical changes occurred in the sample, the signal at 24,350 eV (i.e., that referring to the edge jump position) has also been recorded.

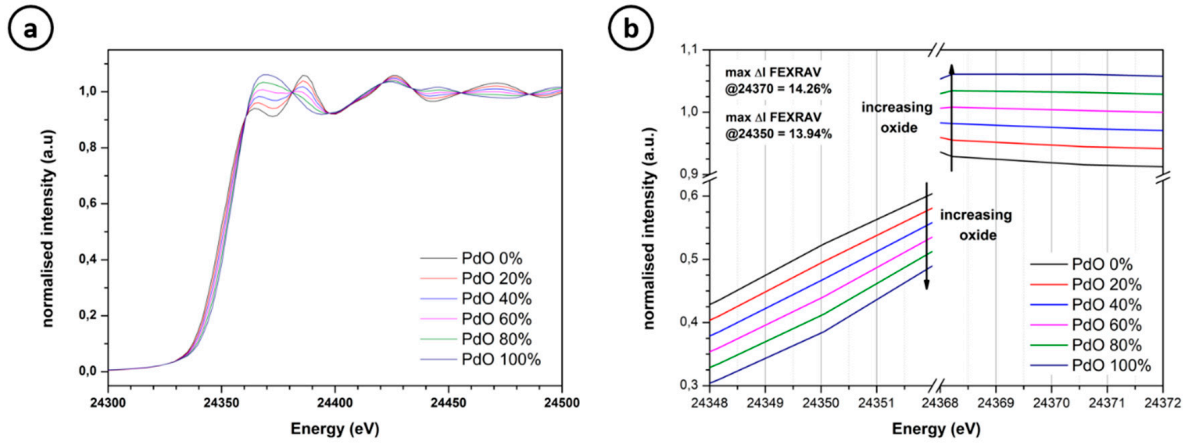

Figure 4. (**a**) Linear combination of X-ray Absorption Near Edge Spectroscopy (XANES) spectra of Pd and PdO with variable molar fraction of PdO; (**b**) The extent of FEXRAV signal variation at 24,370 and 24,390 eV.

The basis for the quantification is that the signal changes linearly depending on the relative change in the Pd concentration. This approach is an extension of the linear combination approach used to fit XANES data for quantification [52]. The key points for FEXRAV quantification are:

(1) The normalised spectral intensity at 24,370 eV decreases linearly with the increase of the Pd(II) content (while at 24,350 eV the trend is opposite, with a decrease of the signal with the increase of Pd(II) content), and

(2) Palladium electrochemical reduction/oxidation occurs through a two-electrons process [53]. Hence, in this context, Palladium speciation varies only between metallic Pd and Pd(II) species (oxides or hydroxypalladiates).

For the two energies proposed, the molar fraction of Pd as derived from the edge at 24,370 and 24,350 eV can be determined with Eqation (1) and Eqation (2) respectively.

$$\%Pd(II)_{(24{,}370\ \mathrm{eV})} = \left(1 - \frac{I_0 - I_{PdO\ (24{,}370\mathrm{eV})}}{I_{Pd\ (24{,}370\ \mathrm{eV})} - I_{PdO\ (24{,}370\ \mathrm{eV})}}\right) * 100 \quad (1)$$

$$\%Pd(II)_{(24{,}350\ \mathrm{eV})} = \left(\frac{I_0 - I_{Pd,\ (24{,}370\ eV)}}{I_{PdO\ (24{,}350\ \mathrm{eV})} - I_{Pd\ (24{,}350\ \mathrm{eV})}}\right) * 100 \quad (2)$$

where $\%Pd(II)_{(energy)}$ is the molar fraction at a certain energy, I_0 is the fluorescence signal of the sample, $I_{Pd\ (energy)}$ and $I_{PdO\ (energy)}$ is the calibrated signal of the Pd and PdO references respectively.

Under the adopted experimental conditions, one can estimate the uncertainty and minimum detection limit from the reproducibility of the intensity of the Fluorescence signal with time. Accordingly, we performed a long acquisition of the noise. Figure 5 shows the changes in the fluorescence signal, along with the average value and ±3σ values. Noise oscillation resulted in the order of 1% of the total fluorescence. This uncertainty is independent on the energy value for energy variations in the 24,300 to 24,400 eV range and can increase relevantly as a reciprocal function of the net change of intensity during the jump. Thus, a reference value of ~1% of the normalised intensity jump can be considered as a limit value for the determination of Pd(II) in FEXRAV. Regarding the Pd(II) moles, this corresponds to a minimum detectable change of ~7%.

Figure 6 shows an example of FEXRAV during voltammetric cycle registered at 24,370 eV. The intensity of the Fluorescence yield increases with increasing the applied potential and decreases with decreasing the potential. Numerous cycles performed on different cells confirm this spectral change to be fully reproducible. Figure 6 also compares the FEXRAV cycle with the conventional voltammetry

carried out simultaneously on the same system. The PdO% label refers to the quantification undertaken using palladium oxide as a standard to obtain the typical Pd(II) XANES curves. Accordingly, the occurrence of a definite potential range where a fraction of Pd(II) oxy(hydroxy)des is stabilised is confirmed. Thus, we performed a calibration of the FEXRAV changes, assuming as a starting point the experimental observation that the Pd/C electrode contains, under the open circuit conditions, a 15% molar fraction of PdO [21]. On the light of the performed evaluation, one can estimate that the Pd(II) content at the electrode ranges between 15 and 38% (38% ± 4% max, calculated from error propagation in Equations (1) and (2)) during a single FEXRAV cycle. The molar fraction achievable step-by-step from the Fluorescence signal, according to the procedure, is represented by the bar between the two graphs (as % Pd(II)) calculated according to the Equations (1) and (2) at 24,370 eV and 24,350 eV, respectively. It is worth mentioning that for the actual catalyst amount that is required for performing the measurements, cyclic voltammetry shows a significant iR drop as only a 70% iR compensation was used to avoid signal instabilities. This effect is ascribed to the fact that we observe currents exceeding 150 mA and that under this condition, a potential shift is due to the residual uncompensated resistance. Additionally, the cyclic voltammetry shows a significant cathodic current at low overpotential. This current is attributed to the presence of dissolved oxygen that was kept in the solution to simulate the real conditions of the fuel in direct ethanol fuel cells.

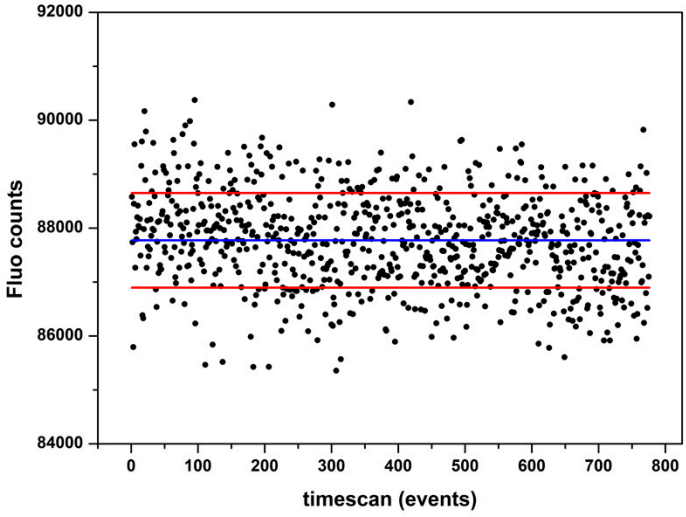

Figure 5. Determination of the noise at the 24,370 eV, the selected energy for the quantification of palladium speciation.

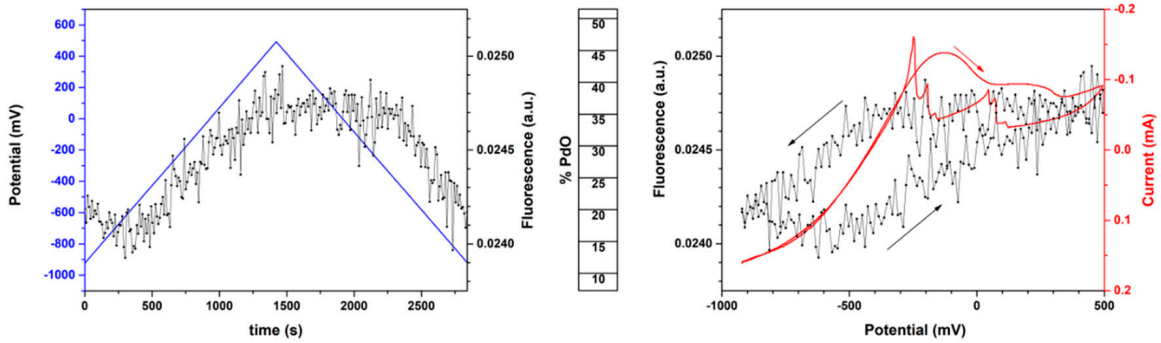

Figure 6. FEXRAV data obtained on the Pd/KOH/EtOH half-cell system at 24,370 eV. Potential scan (blue line) and Fluorescence signal (black line) versus time (Left Figure); Cyclic voltammetry (red line) and Fluorescence signal (black line) versus the applied potential (in the right Figure). Between the Figures, the scale indicating the molar fraction of Pd(II) evaluated according to the procedure described in the text.

3. Materials and Methods

3.1. Chemicals and Catalyst Preparation

A 1 M KOH (Fluka, Munich, Germany) + EtOH 1 M (AnalaR Normapur 99.9%, VWR Chemicals, Milan, Italy) solution was used as electrolyte during voltammetric tests. The solution was deaerated before its introduction inside the cell. Then, the cell kept under nitrogen environment during the whole experimental acquisition.

The Pd on C catalyst was prepared according to the procedure described elsewhere [21]. The synthesis of a batch of catalysts starts with the suspension of 6.0 g of Vulcan XC-72 in 250 mL flask of ethylene glycol, followed by 20 min sonication. Then a mixture of MilliQ water (50 mL), ethylene glycol (50 mL, Sigma-Aldrich, anhydrous 99.8%) and 20 mL HCl (Sigma-Aldrich, reagent grade, 37%, (Milan, Italy) with 2 g of $PdCl_2$ (Sigma-Aldrich, Reagent plus, (Milan, Italy) is added drop by drop under an N_2 stream. After stirring, an alkaline solution of NaOH (13.2 g, Sigma-Aldrich, (Milan, Italy) in H_2O (10 mL) and ethylene glycol (35 mL) was introduced in a closed reactor, which then was heated at 140 °C for three h again under an N_2 atmosphere. After cooling, the solid product was filtered and washed with H_2O to neutral pH. The final product was dried in a vacuum oven at 40 °C. 7.79 g of catalyst was obtained, the total Pd content being determined in 20.3 wt. % [54]. All the solutions were freshly prepared with Milli-Q water (18.2 MΩ cm).

3.2. Beamline Set-Up

Experiments were conducted at the BM-08 LISA CRG Beamline at the European Synchrotron Radiation Facility (ESRF) (see affiliations) in Grenoble [55] during four experimental sessions (08-01-996, MA2936, MA3173, and MA3431, in chronological order). For the first three sessions, a dynamically focusing sagittal monochromator equipped with a pair of Si(311) crystals were employed [45]. During experiment MA3431, samples were measured after the first part of the BM08 refurbishment [55] using a pair of flat Si [311] monochromator crystals. In all experimental sessions, a pair of Pt-coated mirrors ($E_{cutoff} \simeq 27$ keV) was used for harmonic rejection and vertical focusing on the sample; beam size on the sample was approximately 2000 μm (H) × 200 μm (V); energy resolution (ΔE/E) was $\approx 10^{-5}$. Measurements were carried out in fluorescence mode by means of a 12-element solid-state (high purity Germanium) detector. All the spectroscopic and electrochemical measurements were synchronised and performed within the SPEC environment (Certified Scientific Software; http://www.certif.com/). The line was also furbished with ion chambers, one measuring the incoming beam (I_0) and the others reading beam transmitted through the sample (I_1) and the reference (I_R). This particular set-up permits both to avoid signal variations due to changes in the incoming photon beam (by simple normalization of the sample signal using I_0) and to calibrate the acquisition energy through the simultaneous analysis of a Pd reference foil, located in a second analytical XAS chamber. The software ATHENA was used to average multiple spectra and extract the normalised absorption edge [56–58].

3.3. Electrochemical Set-Up

Experiments were performed using the electrochemical cell described in the result and discussion section. In order to coordinate the application of the required electrochemical conditions together with XAS data acquisition, cyclic voltammetries were recorded with a PAR 263 potentiostat that was interfaced with SPEC, exploiting a well-established setup at ESRF [47,48]. A standard Ag/AgCl KCl Sat. electrode has been employed as RE. The CE was a graphite rod. Voltammetries were performed using a scan speed of 1 mV/s. All the potentials of this study are quoted against the reversible hydrogen electrode (RHE) potential scale. Moreover, the potential window in which to perform voltammetries was selected in such a way that a little superimposition with the oxygen evolution region happened. The cell configuration also allowed easy removal of possible bubbles through an open channel in the upper part of the cell, thanks to an electrodic surface orthogonal to the floor plan.

3.4. SEM, TEM and XRD Acquisitions

A Tescan Gaia 3 FIB/SEM (Brno, Czech Republic) was used to acquire the images, using the built-in annular backscattered electrons (BSE) detector. Images were collected using a 15 keV energy for the electron beam. TEM images were acquired using a Philips CM 12 microscope.

X-ray diffraction patterns were acquired at room temperature with a PANalytical X'PERT PRO diffractometer (Malvern, UK), employing CuKα radiation (λ = 1.54187 Å) and a parabolic MPD mirror. The spectra were acquired in the 2θ range from 20° to 80°.

4. Conclusions

In this work, we have successfully demonstrated the application of FEXRAV to the quantification of the speciation of palladium in-situ, for a given sample with a defined particle distribution. Besides the quantification approach, we have built up a new cell design that allows the acquisition of XAS data in Fluorescence mode and avoids the use of flow systems, overcoming two major limitations: (i) Flow systems are usually difficult to fit in the measurement XAS chamber and (ii) they cannot simulate the conditions that are commonly encountered in passive fuel cells. With the cell, we have identified the suitable conditions to perform FEXRAV on carbon black supported Pd electrocatalysts, defining the parameters that a sample must meet to allow a reliable quantification.

Our data show that FEXRAV allows the quantification of the catalyst speciation under dynamic conditions, with a time resolution that for our experimental set-up was 4s. Additionally, we have investigated the noise to determine the lower detection limit of quantitative FEXRAV. We found that a cyclic voltammetry scan performed between 0.2 and 1.5 V at a scan rate of 1 mV s^{-1} produces a maximum Pd(II) content of 38% in mole fraction.

Quantitative FEXRAV enables the quantitative determination of the oxidation of electrocatalysts that is a primary cause of the degradation of the performance of electrochemical energy conversion devices. This knowledge has a tremendous impact in designing mitigation strategies to boost the service life of catalysts and devices.

Author Contributions: E.B. (Paper writing, ESRF experiments participation), A.G. (Paper writing, ESRF experiment participation, data analysis), G.M. (Paper writing, Experiment design, ESRF experiments participation), F.D. (ESRF experiments participation), F.D.B. (Paper writing, Experiment design, ESRF experiments participation, data analysis), C.Z. (ESRF experiments participation), A.P. (ESRF experiments participation), G.O.L. (ESRF experiments participation), H.M. (Catalyst synthesis), W.G. (Data analysis), M.I. (advice on the systems to be investigated), F.V. (advice on the systems to be investigated) and A.L. (Paper writing, ESRF experiments participation, electrochemical cell design, e).

Funding: "Ente Cassa di Risparmio di Firenze" with the projects: "Richiesta contributo per acquisto di un microscopio elettronico a scansione ad ultra-alta risoluzione per potenziare il Centro di Microscopie Elettroniche (Ce.M.E.) and "EnergyLab"; POR FESR 2014-2020 project FELIX (Fotonica ed Elettronica Integrate per l'Industria), project code n. 6455; PRIN 2017 project funded by the Italian Ministry for University and Research (MIUR) (grant n. 2017YH9MRK).

Acknowledgments: The authors gratefully acknowledge the Italian National Research Council (CNR) microscopy facility "Ce.M.E.—Centro Microscopie Elettroniche Laura Bonzi" for the SEM images, and the CNR-ICCOM technician Carlo Bartoli for the electrochemical cell manufacturing. ESRF is gratefully acknowledged for the provision of synchrotron radiation during the MA3431, MA3173, MA2936, and 08-01-996 experiments carried out at the Italian LISA BM08 beamline. Francesco Carlà (former scientist of ID03), is also acknowledged for the access to the ESRF electrochemistry lab.

Conflicts of Interest: The authors declare no conflict of interest.

References

1. Meirer, F.; Weckhuysen, B.M. Spatial and temporal exploration of heterogeneous catalysts with synchrotron radiation. *Nat. Rev. Mater.* **2018**, *3*, 324–340. [CrossRef]
2. Fabbri, E.; Abbott, D.F.; Nachtegaal, M.; Schmidt, T.J. Operando X-ray absorption spectroscopy: A powerful tool toward water splitting catalyst development. *Curr. Opin. Electrochem.* **2017**, *5*, 20–26. [CrossRef]

3. Frenkel, A.I.; Rodriguez, J.A.; Chen, J.G. Synchrotron techniques for in situ catalytic studies: Capabilities, challenges, and opportunities. *ACS Catal.* **2012**, *2*, 2269–2280. [CrossRef]
4. Fracchia, M.; Ghigna, P.; Vertova, A.; Rondinini, S. Time-Resolved X-ray Absorption Spectroscopy in (Photo) Electrochemistry Time-Resolved X-ray Absorption Spectroscopy in (Photo) Electrochemistry. *Surfaces* **2018**, *1*, 138–150. [CrossRef]
5. Koningsberger, D.C.; Mojet, B.L.; van Dorssen, G.E.; Ramaker, D.E. XAFS spectroscopy; fundamental principles and data analysis. *Top. Catal.* **2000**, *10*, 143–155. [CrossRef]
6. Sharma, A.; Singh, J.; Won, S.O.; Chae, K.; Sharma, S.K.; Kumar, S. Introduction to X-Ray Absorption Spectroscopy and Its Applications in Material Science. In *Handbook of Materials Characterization*; Sharma, S., Ed.; Springer: Cham, Switzerland, 2018; pp. 497–548.
7. Niwa, H.; Horiba, K.; Harada, Y.; Oshima, M.; Ikeda, T.; Terakura, K.; ichi Ozaki, J.; Miyata, S. X-ray absorption analysis of nitrogen contribution to oxygen reduction reaction in carbon alloy cathode catalysts for polymer electrolyte fuel cells. *J. Power Sources* **2009**, *187*, 93–97. [CrossRef]
8. Friebel, D.; Miller, D.J.; O'Grady, C.P.; Anniyev, T.; Bargar, J.; Bergmann, U.; Ogasawara, H.; Wikfeldt, K.T.; Pettersson, L.G.M.; Nilsson, A. In situ X-ray probing reveals fingerprints of surface platinum oxide. *Phys. Chem. Chem. Phys.* **2011**, *13*, 262–266. [CrossRef]
9. McBreen, J. The application of synchrotron techniques to the study of lithium-ion batteries. *J. Solid State Electrochem.* **2009**, *13*, 1051–1061. [CrossRef]
10. Erickson, E.M.; Thorum, M.S.; Vasić, R.; Marinković, N.S.; Frenkel, A.I.; Gewirth, A.A.; Nuzzo, R.G. In situ electrochemical X-ray absorption spectroscopy of oxygen reduction electrocatalysis with high oxygen flux. *J. Am. Chem. Soc.* **2012**, *134*, 197–200. [CrossRef]
11. Friebel, D.; Louie, M.W.; Bajdich, M.; Sanwald, K.E.; Cai, Y.; Wise, A.M.; Cheng, M.-J.; Sokaras, D.; Weng, T.-C.; Alonso-Mori, R.; et al. Identification of highly active Fe sites in (Ni,Fe)OOH for electrocatalytic water splitting. *J. Am. Chem. Soc.* **2015**, *137*, 1305–1313. [CrossRef]
12. Zitolo, A.; Ranjbar-Sahraie, N.; Mineva, T.; Li, J.; Jia, Q.; Stamatin, S.; Harrington, G.F.; Lyth, S.M.; Krtil, P.; Mukerjee, S.; et al. Identification of catalytic sites in cobalt-nitrogen-carbon materials for the oxygen reduction reaction. *Nat. Commun.* **2017**, *8*, 1–10. [CrossRef] [PubMed]
13. Ginder-Vogel, M.; Landrot, G.; Fischel, J.S.; Sparks, D.L. Quantification of rapid environmental redox processes with quick-scanning x-ray absorption spectroscopy (Q-XAS). *Proc. Natl. Acad. Sci. USA* **2009**, *106*, 16124–16128. [CrossRef]
14. Minguzzi, A.; Lugaresi, O.; Locatelli, C.; Rondinini, S.; D'Acapito, F.; Achilli, E.; Ghigna, P. Fixed energy X-ray absorption voltammetry. *Anal. Chem.* **2013**, *85*, 7009–7013. [CrossRef] [PubMed]
15. Rondinini, S.; Lugaresi, O.; Achilli, E.; Locatelli, C.; Minguzzi, A.; Vertova, A.; Ghigna, P.; Comninellis, C. Fixed Energy X-ray Absorption Voltammetry and Extended X-ray Absorption fine Structure of Ag nanoparticle electrodes. *J. Electroanal. Chem.* **2016**, *766*, 71–77. [CrossRef]
16. Rondinini, S.; Minguzzi, A.; Achilli, E.; Locatelli, C.; Agostini, G.; Pascarelli, S.; Spinolo, G.; Vertova, A.; Ghigna, P. The dynamics of pseudocapacitive phenomena studied by Energy Dispersive X-Ray Absorption Spectroscopy on hydrous iridium oxide electrodes in alkaline media. *Electrochim. Acta* **2016**, *212*, 247–253. [CrossRef]
17. D'acapito Francesco, D.R. De LISA Beamline (BM08-ESRF) Annual Report 2016. Available online: https://www.researchgate.net/publication/313161233_LISA_annual_report_2016 (accessed on 2 June 2019).
18. Minguzzi, A.; Ghigna, P.; Rondinini, S.; Chimica, D.; Golgi, V. α- and γ-FeOOH: Stability, Reversibility, and Nature of the Active Phase under Hydrogen Evolution. *ACS Appl. Energy Mater.* **2018**, *1*, 1716–1725.
19. Antolini, E. Palladium in fuel cell catalysis. *Energy Environ. Sci.* **2009**, *2*, 915. [CrossRef]
20. Liang, Z.X.; Zhao, T.S.; Xu, J.B.; Zhu, L.D. Mechanism study of the ethanol oxidation reaction on palladium in alkaline media. *Electrochim. Acta* **2009**, *54*, 2203–2208. [CrossRef]
21. Miller, H.A.; Lavacchi, A.; Vizza, F.; Marelli, M.; Di Benedetto, F.; D'Acapito, F.; Paska, Y.; Page, M.; Dekel, D.R. A Pd/C-CeO2 Anode Catalyst for High-Performance Platinum-Free Anion Exchange Membrane Fuel Cells. *Angew. Chem. Int. Ed. Engl.* **2016**, *55*, 6004–6007. [CrossRef]
22. Tsui, L.K.; Zafferoni, C.; Lavacchi, A.; Innocenti, M.; Vizza, F.; Zangari, G. Electrocatalytic activity and operational stability of electrodeposited Pd-Co films towards ethanol oxidation in alkaline electrolytes. *J. Power Sources* **2015**, *293*, 815–822. [CrossRef]

23. Wang, L.; Bambagioni, V.; Bevilacqua, M.; Bianchini, C.; Filippi, J.; Lavacchi, A.; Marchionni, A.; Vizza, F.; Fang, X.; Shen, P.K. Sodium borohydride as an additive to enhance the performance of direct ethanol fuel cells. *J. Power Sources* **2010**, *195*, 8036–8043. [CrossRef]
24. Bianchini, C.; Shen, P.K. Palladium-Based Electrocatalysts for Alcohol Oxidation in Half Cells and in Direct Alcohol Fuel Cells. *Chem. Rev.* **2009**, *109*, 4183–4206. [CrossRef] [PubMed]
25. Chen, Y.; Bellini, M.; Bevilacqua, M.; Fornasiero, P.; Lavacchi, A.; Miller, H.A.; Wang, L.; Vizza, F. Direct Alcohol Fuel Cells: Toward the Power Densities of Hydrogen-Fed Proton Exchange Membrane Fuel Cells. *ChemSusChem* **2014**, *8*, 524–533. [CrossRef] [PubMed]
26. Moraes, L.P.R.; Matos, B.R.; Radtke, C.; Santiago, E.I.; Fonseca, F.C.; Amico, S.C.; Malfatti, C.F. Synthesis and performance of palladium-based electrocatalysts in alkaline direct ethanol fuel cell. *Int. J. Hydrog. Energy* **2016**, *41*, 6457–6468. [CrossRef]
27. Chen, Y.X.; Lavacchi, A.; Miller, H.A.; Bevilacqua, M.; Filippi, J.; Innocenti, M.; Marchionni, A.; Oberhauser, W.; Wang, L.; Vizza, F. Nanotechnology makes biomass electrolysis more energy efficient than water electrolysis. *Nat. Commun.* **2014**, *5*, 4036. [CrossRef] [PubMed]
28. Bambagioni, V.; Bianchini, C.; Chen, Y.; Filippi, J.; Fornasiero, P.; Innocenti, M.; Lavacchi, A.; Marchionni, A.; Oberhauser, W.; Vizza, F. Energy Efficiency Enhancement of Ethanol Electrooxidation on Pd–CeO_2/C in Passive and Active Polymer Electrolyte-Membrane Fuel Cells. *ChemSusChem* **2012**, *5*, 1266–1273. [CrossRef] [PubMed]
29. Grdeń, M.; Łukaszewski, M.; Jerkiewicz, G.; Czerwiński, A. Electrochemical behaviour of palladium electrode: Oxidation, electrodissolution and ionic adsorption. *Electrochim. Acta* **2008**, *53*, 7583–7598. [CrossRef]
30. Wang, L.; Lavacchi, A.; Bellini, M.; D'Acapito, F.; Di Benedetto, F.; Innocenti, M.; Miller, H.A.; Montegrossi, G.; Zafferoni, C.; Vizza, F. Deactivation of Palladium Electrocatalysts for Alcohols Oxidation in Basic Electrolytes. *Electrochim. Acta* **2015**, *177*, 100–106. [CrossRef]
31. Montegrossi, G.; Giaccherini, A.; Berretti, E.; Di Benedetto, F.; Innocenti, M.; D'Acapito, F.; Lavacchi, A. Computational speciation models: A tool for the interpretation of spectroelectrochemistry for catalytic layers under operative conditions. *J. Electrochem. Soc.* **2017**, *164*, 3690–3695. [CrossRef]
32. Grdeń, M. Electrochemical quartz crystal microbalance studies of a palladium electrode oxidation in a basic electrolyte solution. *Electrochim. Acta* **2009**, *54*, 909–920. [CrossRef]
33. Grdeń, M.; Kotowski, J.; Czerwiński, A. The study of electrochemical palladium behavior using the quartz crystal microbalance. *J. Solid State Electrochem.* **2000**, *4*, 273–278. [CrossRef]
34. Ayyappan, S.; Srinivasa Gopalan, R.; Subbanna, G.N.; Rao, C.N.R. Nanoparticles of Ag, Au, Pd, and Cu produced by alcohol reduction of the salts. *J. Mater. Res.* **1997**, *12*, 398–401. [CrossRef]
35. Nguyen, V.L.; Nguyen, D.C.; Hirata, H.; Ohtaki, M.; Hayakawa, T.; Nogami, M. Chemical synthesis and characterization of palladium nanoparticles. *Adv. Nat. Sci. Nanosci. Nanotechnol.* **2010**, *1*, 035012. [CrossRef]
36. Asset, T.; Serov, A.; Padilla, M.; Roy, A.J.; Matanovic, I.; Chatenet, M.; Maillard, F.; Atanassov, P. Design of Pd-Pb Catalysts for Glycerol and Ethylene Glycol Electrooxidation in Alkaline Medium. *Electrocatalysis* **2018**, *9*, 480–485. [CrossRef]
37. Lenarda, A.; Bellini, M.; Marchionni, A.; Miller, H.A.; Montini, T.; Melchionna, M.; Vizza, F.; Prato, M.; Fornasiero, P. Nanostructured carbon supported Pd-ceria as anode catalysts for anion exchange membrane fuel cells fed with polyalcohols. *Inorg. Chim. Acta* **2018**, *470*, 213–220. [CrossRef]
38. Marchionni, A.; Bevilacqua, M.; Bianchini, C.; Chen, Y.-X.; Filippi, J.; Fornasiero, P.; Lavacchi, A.; Miller, H.; Wang, L.; Vizza, F. Electrooxidation of Ethylene Glycol and Glycerol on Pd-(Ni-Zn)/C Anodes in Direct Alcohol Fuel Cells. *ChemSusChem* **2013**, *6*, 518–528. [CrossRef] [PubMed]
39. Simões, M.; Baranton, S.; Coutanceau, C. Electro-oxidation of glycerol at Pd based nano-catalysts for an application in alkaline fuel cells for chemicals and energy cogeneration. *Appl. Catal. B Environ.* **2010**, *93*, 354–362. [CrossRef]
40. Garcia, A.C.; Birdja, Y.Y.; Tremiliosi-Filho, G.; Koper, M.T.M. Glycerol electro-oxidation on bismuth-modified platinum single crystals. *J. Catal.* **2017**, *346*, 117–124. [CrossRef]
41. Yasuhiro, I.; Kiyotaka, A.; Mizuki, T. (Eds.) "Reflection XAFS". In *XAFS Techniques for Catalysts, Nanomaterials, and Surfaces*; Springer International Publishing: Cham, Switzerland, 2017. [CrossRef]
42. Arblaster, J.W. Crystallographic Properties of Palladium. *Platin. Met. Rev.* **2013**, *57*, 127–136. [CrossRef]

43. Achilli, E.; Minguzzi, A.; Visibile, A.; Locatelli, C. short communications 3D-printed photo-spectroelectrochemical devices for in situ and in operando X-ray absorption spectroscopy investigation. *J. Synchrotron. Radiat.* **2016**, *23*, 622–628. [CrossRef]
44. Henke, B.L.; Gullikson, E.M.; Davis, J.C. X-Ray Interactions: Photoabsorption, Scattering, Transmission, and Reflection at E = 50-30,000 eV, Z = 1-92. *At. Data Nucl. Data Tables* **1993**, *54*, 181–342. [CrossRef]
45. Grden, M.; Czerwinski, A. EQCM studies on Pd—Ni alloy oxidation in basic solution. *J. Solid State Electrochem.* **2008**, *12*, 375–385. [CrossRef]
46. Cookson, B.J. The Preparation of Palladium Nanoparticles. *Plat. Met. Rev.* **2012**, *56*, 83–98. [CrossRef]
47. Kim, Y.; Kim, J.; Kim, D.H. Investigation on the enhanced catalytic activity of a Ni-promoted Pd/C catalyst for formic acid dehydrogenation: Effects of preparation methods and Ni/Pd ratios. *RSC Adv.* **2018**, *8*, 2441–2448. [CrossRef]
48. Waser, J.; Levy, H.A.; Peterson, S.W. The structure of PdO. *Acta Crystallogr.* **1953**, *6*, 661–663. [CrossRef]
49. Moore, W.J.; Pauling, L. The Crystal Structures of the Tetragonal Monoxides of Lead, Tin, Palladium, and Platinum. *J. Am. Chem. Soc.* **1941**, *63*, 1392–1394. [CrossRef]
50. Greenwood, N.N.; Earnshaw, A. *Chemistry of the Elements*; Elsevier: Amsterdam, The Netherlands, 1997; ISBN 9780750633659.
51. Torapava, N.; Elding, L.I.; Mändar, H.; Roosalu, K.; Persson, I. Structures of polynuclear complexes of palladium(ii) and platinum(ii) formed by slow hydrolysis in acidic aqueous solution. *Dalton Trans.* **2013**, *42*, 7755–7760. [CrossRef] [PubMed]
52. Bardelli, F.; Veronesi, G.; Capella, S.; Bellis, D.; Charlet, L.; Cedola, A.; Belluso, E. New insights on the biomineralisation process developing in human lungs around inhaled asbestos fibres. *Sci. Rep.* **2017**, *7*, 44862. [CrossRef] [PubMed]
53. Griffith, W.P.; Robinson, S.D.; Swars, K. *Pd Palladium: Palladium Compounds*; Griffith, W.P., Swars, K., Eds.; Springer: Berlin/Heidelberg, Germany, 1989; ISBN 978-3-662-09190-6.
54. Vayenas, C.G.; White, R.E. *Modern Aspects of Electrochemistry 51*; Springer International Publishing: Basel, Switzerland, 2011.
55. d'Acapito, F.; Lepore, G.O.; Puri, A.; Laloni, A.; La Mannna, F.; Dettona, E.; De Luisa, A.; Martin, A. The LISA beamline at ESRF. *J. Synchrotron. Radiat.* **2019**, *26*, 551–558. [CrossRef]
56. Ravel, B.; Newville, M. ATHENA, ARTEMIS, HEPHAESTUS: Data analysis for X-ray absorption spectroscopy using IFEFFIT. *J. Synchrotron. Radiat.* **2005**, *12*, 537–541. [CrossRef] [PubMed]
57. Giaccherini, A.; Cinotti, S.; Guerri, A.; Carlà, F.; Montegrossi, G.; Vizza, F.; Lavacchi, A.; Felici, R.; Di Benedetto, F.; Innocenti, M. Operando SXRD study of the structure and growth process of Cu2S ultra-thin films. *Sci. Rep.* **2017**, *7*, 1615. [CrossRef] [PubMed]
58. Giaccherini, A.; Russo, F.; Carlà, F.; Guerri, A.; Picca, R.A.; Cioffi, N.; Cinotti, S.; Montegrossi, G.; Passaponti, M.; Di Benedetto, F.; et al. Operando SXRD of E-ALD deposited sulphides ultra-thin films: Crystallite strain and size. *Appl. Surf. Sci.* **2018**, *432*, 53–59. [CrossRef]